Infiltration of Fibrous Preforms by a Pure Metal: Part II. Experiment

L.J. MASUR, A. MORTENSEN, J.A. CORNIE, and M.C. FLEMINGS

In a previous paper, a theory was developed to describe the flow of a pure metal into a fibrous preform. This paper presents experimental data to test the results of the theory for pure aluminum flowing into fibrous alumina preforms. An apparatus was designed and built for unidirectional infiltration under constant pressure and carefully controlled temperature parameters. A sensor was also developed to measure the position of the liquid metal in the fibrous preform during the experiment. This technique enabled quantitative comparison of theory and experiment. Experimental data are reported for the infiltration by 99.999 and 99.9 wt pct pure aluminum of SAFFIL alumina fibers fabricated into two-dimensionally random preforms. Fiber volume fraction was varied from 0.22 to 0.26, fiber preheat temperature was varied from approximately 483 to 743 K, and metal superheat was varied from 20 to 185 K. Infiltration pressure was varied from 1 to 4.5 MPa (145 to 650 psi). Agreement between theory and experiment was very good under all the experimental conditions studied for the 99.999 wt pct pure matrix. The impurity level of the metal was found to influence infiltration significantly. The measured preform permeability for 99.9 wt pct aluminum was much lower than that for 99.999 wt pct aluminum.

I. INTRODUCTION

IN a previous paper,[1] analytical solutions were given to describe the unidirectional infiltration of a pure metal into a preform of aligned fibers under the application of a constant pressure. In particular, the influence on infiltration kinetics was shown for the processing parameters, including (a) fiber volume fraction, (b) fiber temperature, (c) metal superheat, and (d) applied pressure. Flow of metal into a fiber preform heated significantly below the metal melting point was shown to result in the solidification of metal around the fibers to form a sheath. Also, it was shown that the effect of metal superheat was to remelt this solid metal sheath at a remelting front separating two regions in the composite. The cessation of fluid flow was shown to be due to solidification from the mold wall progressing inward and closing the flow channel. Calculations were performed to predict the behavior of pure aluminum infiltrating alumina fibers in cross flow under a variety of experimental conditions.

In this paper, experiments are presented to test the results of the foregoing analysis. All experiments were performed with alumina fibers and aluminum metal. The experiments reported here were performed with the fibers initially at a temperature significantly below the metal melting point. This is the case of practical interest for the fabrication of many fiber-reinforced metal components, including, for example, diesel engine pistons.

L.J. MASUR, formerly a Graduate Student with the Department of Materials Science and Engineering, Massachusetts Institute of Technology, is Senior Scientist with the American Superconductor Corporation, Cambridge, MA 02139. A. MORTENSEN, Assistant Professor, J.A. CORNIE, Principal Research Associate, and M.C. FLEMINGS, Professor and Department Head, are with the Department of Materials Science and Engineering, Massachusetts Institute of Technology, Cambridge, MA 02139.

Manuscript submitted June 7, 1988.

II. EXPERIMENTAL APPARATUS AND PROCEDURE

A. *Fiber Preform Preparation*

SAFFIL* fibers were obtained from Imperial Chemical Industries, London, England. SAFFIL is a nominally 3-μm-diameter, delta-alumina fiber that is chopped and pressed into disk-shaped preforms. The preform fabrication operation tends to align the fiber axes perpendicular to the pressing direction, resulting in a two-dimensional random arrangement of fibers. The preforms used in this study were 100 mm in diameter by 15-mm thick and featured a nominal fiber density of 24 vol pct.

*SAFFIL is a trademark of ICI Americas, Inc., Wilmington, DE.

Cylindrical plugs were cut from the mother preform using a knife-edged cutter 17 mm in internal diameter. These plugs were then tightly fitted into quartz tubes 17 mm in internal diameter and 1 mm in wall thickness. Their orientation was such that metal infiltration was perpendicular to the fiber axes. In these experiments, either two or three plugs were placed atop one another within the quartz tube, resulting in fiber preforms 30 or 45 mm in length. Each plug cut from the preform was weighed to calculate fiber volume fraction; the plugs in any given experiment were always within 0.5 fiber vol pct of one another. A ceramic support rod was placed on top of the preforms to prevent them from moving upward in the quartz tube during infiltration. Figure 1 schematically illustrates the preform preparation process.

Selected preforms (chosen at random for each batch of raw materials) were further characterized by a water permeability test. In this test, a falling head permeability apparatus[2] was used to measure the permeability of the preform to flowing water.

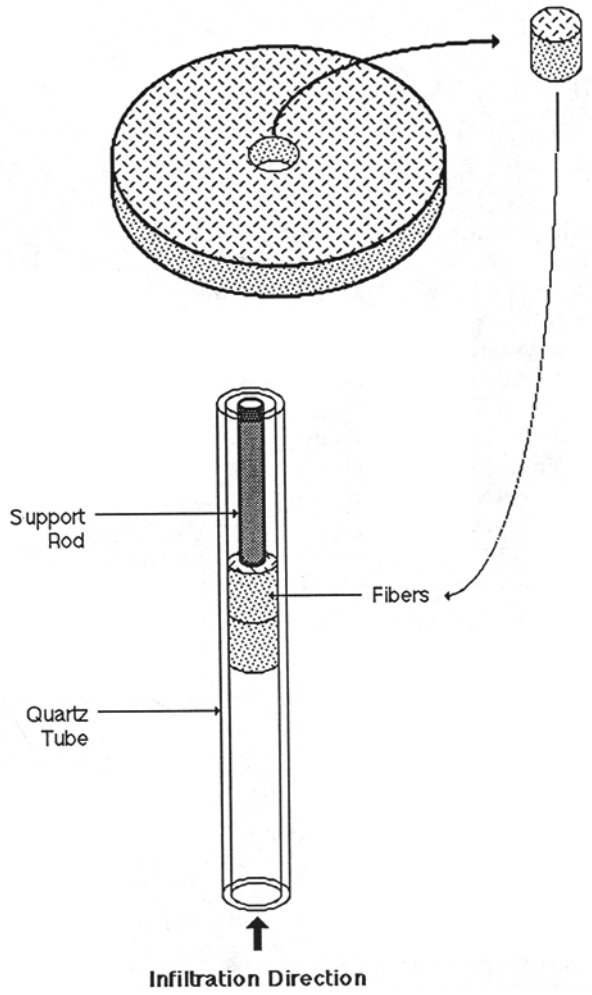

Fig. 1 — Schematic drawing of fiber preform preparation process.

B. *Pressure Infiltration Apparatus*

Figure 2 is a schematic drawing of the pressure casting apparatus that was constructed for this study. The fiber-filled quartz tube discussed above was secured to the cap of the apparatus with an O-ring fitting, above which was attached a stainless steel tube to act as a chill in the event of overinfiltration. The fibers were heated by a helically wound resistance heater consisting of a 3.2-mm-diameter sheathed heating element wound around, and silver-soldered to, a 15.2-cm-long steel cylinder (1.6-mm wall thickness). The heater assembly was placed over the quartz tube in the vicinity of the fibers; the space between the heater and quartz was filled by a 1.6-mm-thick layer of FIBERFRAX* insulation. Temperature control was maintained with a thermocouple placed between the quartz tube and the heater at the midpoint of the fiber preform length. Temperature differences measured within the furnace over the 45-mm length occupied by the fibers were found not to vary by more than ±3 K.

A second resistance furnace for metal melting was located in the bottom of the pressure vessel portion of the pressure casting apparatus. It measured 11.4 cm in internal diameter and 15.2 cm in height. Metal, either 99.9 or 99.999 wt pct aluminum, was melted in a thick-walled graphite crucible in air to preserve metal purity.

*FIBERFRAX is a trademark of Standard Oil Engineered Materials Co., Niagara Falls, NY.

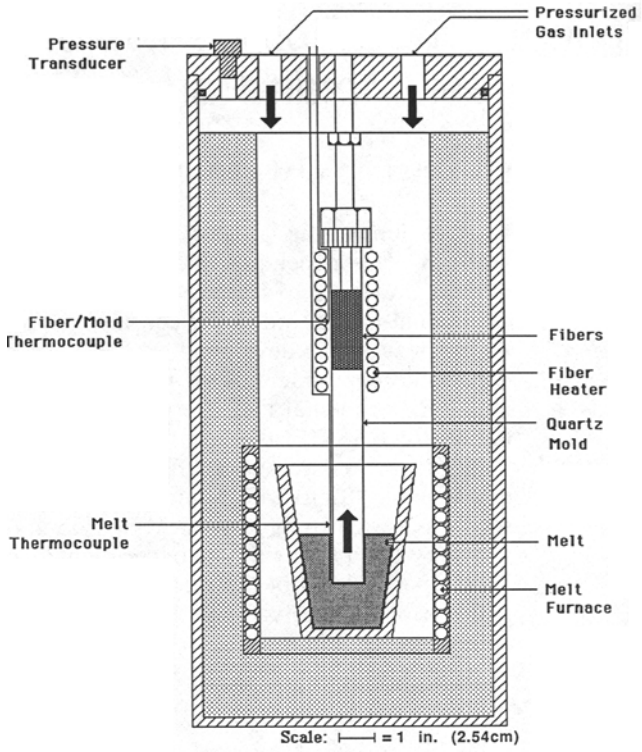

Fig. 2 — Schematic drawing of pressure casting apparatus.

Pressurization was achieved with nitrogen gas, which was delivered to the apparatus through two inlets *via* two 10.2-mm internal-diameter high-pressure hoses. Fast pressurization of the apparatus (≈1.2 seconds) was achieved by prepressurizing a holding tank, from which nitrogen was released *via* two 10.2-mm orifice ball valves. Thus, the infiltration experiments were conducted at constant pressure over most of their duration, typically of about 10 seconds. This feature of the procedure, combined with the unidirectionality of infiltration, enabled us to use results from calculations presented in Reference 1 to interpret the data.

Compression experiments were performed on the uninfiltrated fiber preform material along the axis of infiltration. These were performed within a heated quartz tube so as to replicate the actual conditions of the infiltration experiments. Strain was measured from crosshead displacement. It was found that preform deformation remained relatively small (<0.03 engineering strain) up to a pressure of about 3.5 MPa, at which the preform started deforming significantly. Therefore, applied pressure was varied from 0 to 3.5 MPa in the infiltration experiments to avoid complications related to preform compression during infiltration. The preform deformation that occurred during infiltration was limited to a strain of only 0.03, which resulted in an imprecision in the volume fraction V_f of less than 0.01.

C. *Liquid Metal Position Sensor*

A technique was developed to sense the position of the liquid metal front as it advances through the fiber

preform during infiltration. An SiC filament and the molten metal were used as a variable resistor, and as a result of its change in resistance during the experiment, the liquid metal position could be calculated. The filament was a 140-μm-diameter SCS-2 SiC fiber manufactured by AVCO-Specialty Materials Division, Lowell, MA. It is very stiff, which is ideal for specimen preparation, and has a relatively high electrical resistivity ($\approx$10 Ω/mm), which is important for resolution of the metal position.

A single SiC filament was inserted through the center of the preform during specimen preparation. The top of the filament above the preform was nickel-plated and attached to the fitting at the top of the quartz tube. The portions of the filament within the preform and extending out the bottom were unplated and allowed to hang free. The interface between the plated and unplated parts of the filament was located exactly at the top of the preform. A load resistor was placed in series with the filament, and a constant potential was applied between the load resistor and the metal crucible, with the molten metal acting as a switch to close the circuit (Figure 3). The potential drop across the SiC filament was recorded as a function of time. As the metal infiltrated the preform, the potential measured across the filament decreased due to the decrease in its effective electrical length, so that by monitoring the potential drop during infiltration, the position of the metal front and its velocity could be determined. Examples of typical infiltration profiles, in terms of infiltration length *vs* time, are given in Figure 4. The final infiltrated length of most samples was measured independently of the SiC filament and found to deviate from that measured with the sensor by no more than 10 pct.

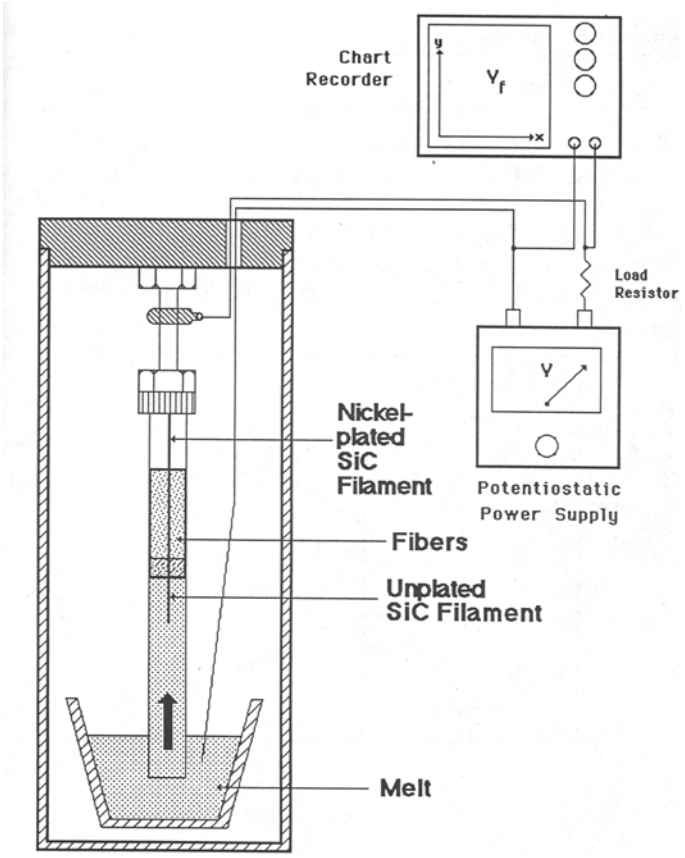

Fig. 3 — Schematic drawing of liquid position measurement technique. An SiC filament detects movement of the liquid metal.

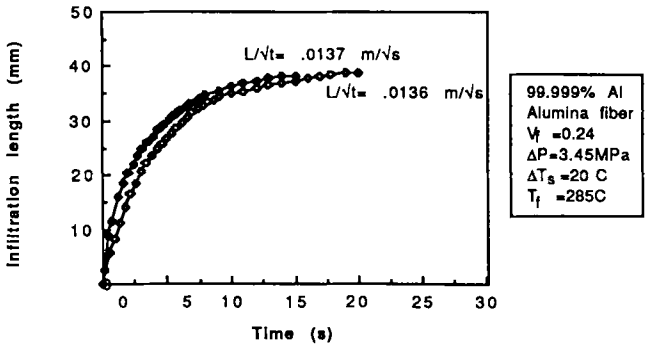

Fig. 4 — Infiltration profiles recorded with the device in Fig. 3 for runs 8 and 9, Table I.

D. *Aluminum-Lead Experiments*

A technique was developed for infiltrating a small amount of aluminum followed by molten lead. In these experiments, 2 to 3 g of aluminum were melted and floated on a bath of molten lead. When the system was subsequently pressurized, a small amount of aluminum preceded the lead into the preform. While the aluminum solidified in the preform during infiltration, the lead flowed into those volumes not occupied by solid aluminum. This provided a high-contrast metallographic observation of the volumes where the aluminum first flowed and solidified, because lead is darker than aluminum under the optical microscope.

E. *Metallographic Examination*

Metallographic preparation of composite samples was achieved by polishing on an automatic polisher with diamond paste on hard synthetic cloth, followed by a final polish with magnesium oxide on a soft billiard-type cloth. Some samples were chemically etched to reveal grains by immersing for 2 to 3 seconds in an etch-pitting solution of 50 ml nitric acid, 47 ml hydrochloric acid, and 3 ml hydrofluoric acid.[3] Observation of the samples under crossed polarizers accentuated the etch pits and readily showed differences in their orientation across different grains.

The purity of the material after infiltration was determined by chemical analyses of samples taken from unreinforced portions of the casting located close to the fiber preform.

III. EXPERIMENTAL RESULTS AND COMPARISON WITH THEORY

A series of 28 infiltration experiments were conducted in this study at various values of pressure, fiber volume fraction, metal superheat, metal purity, and fiber temperature. Experimental conditions are listed in Table I along with measured results.

The total length of flow into the preform, L_f in Table I, was determined from measurement on longitudinally sliced

Table I. Summary of Experiments with Pure Aluminum

Run Number	Nominal Metal Purity	Mold Radius (mm)	V_f	T_f (K)	ΔP_T (MPa)	T_0 (K)	$L\sqrt{t} = \psi$ (m/$\sqrt{s}$)	L_f (mm)	Metal Purity after Experiment (when Analyzed)
1	3N	5.5	0.245	1023	0.72	1023	—	0	—
2	3N	5.5	0.250	983	0.46	983	—	0	—
3	3N	5.5	0.250	973	0.26	973	—	0	—
4	3N	5.5	0.250	603	3.59	960	*	23.0	—
5	3N	8.5	0.250	603	3.52	955	0.0144	43.5	—
6	3N	8.5	0.250	575	3.55	959	0.0113	33.5	—
7	3N	8.5	0.240	559	3.42	951	0.0101	20.5	—
8	5N	8.5	0.240	560	3.48	953	0.0137	38.5	99.990 pct
9	5N	8.5	0.240	562	3.48	951	0.0136	39.0	—
10	5N	8.5	0.240	546	3.52	950	0.0129	33.0	—
11	5N	8.5	0.240	530	3.52	953	0.0115	29.5	99.991 pct
12	5N	8.5	0.240	504	3.45	950	*	22.0	—
13	5N	8.5	0.240	741	3.45	948	0.0304	>45	99.987 pct
14	5N	8.5	0.240	483	3.42	943	0.0051	11.5	—
15	5N	8.5	0.240	645	3.45	948	0.0201	>45	99.990 pct
16	5N	8.5	0.235	528	3.42	1180	0.0147	37.0	—
17	5N	8.5	0.245	528	3.31	1011	0.0104	23.0	99.947 pct
18	5N	8.5	0.240	527	3.45	1073	0.0125	33.0	—
19	5N	8.5	0.235	528	3.42	1023	0.0121	30.0	—
20	5N	8.5	0.220	484	3.45	953	0.0144	36.5	—
21	5N	8.5	0.240	558	2.35	953	0.0100	29.0	—
22	5N	8.5	0.240	558	1.30	953	0.0052	10.5	—
23	5N	8.5	0.260	528	3.38	953	0.0070	14.5	—
24	5N	8.5	0.220	529	3.38	956	0.0158	45.0	—
25	5N	8.5	0.240	562	2.28	950	0.0119	34.5	—
26	5N	8.5	0.240	558	4.52	951	0.0141	39.5	—
27	5N	8.5	0.245	560	0.90	948	*	4.0	—
28	5N	8.5	0.240	557	1.73	952	0.0079	21.0	—

3N indicates starting purity of 99.9 pct.
5N indicates starting purity of 99.999 pct.
*Indicates insufficiently long linear portion on L *vs* $\sqrt{t}$ curve for accurate measurement of slope.

samples. The parameter $L/\sqrt{t} = \psi$, introduced in Reference 1, is also listed. It was determined as described below.

For each run, data such as those in Figure 4 were replotted as L *vs* $\sqrt{t}$, as shown in Figure 5. In these plots, there was invariably an initial transient of about 1 second during which the slope increased (region I in Figure 5). We attribute this to the transient pressure buildup in the chamber. Following this initial transient, a region II was generally observed in which the slope was constant; lastly, in region III, the slope was observed to decrease with time.

Data for $L/\sqrt{t}$ in Table I represent the slope of curves in region II such as that in Figure 5. This was taken to be the value of $L/\sqrt{t} = \psi$ measured after the steady-state pressure level was reached, but before sufficient solidification from external heat loss occurred to significantly affect flow.

The pressure differential, which drives flow of the metal into the preform, was defined in our previous paper[1] as $\Delta P_\mu = P_T - P_g - \Delta P_\gamma$, where P_T is the applied pressure at the entrance of the preform, P_g is the ambient pressure in the preform at the infiltration front, and ΔP_γ is the pressure drop in the liquid metal due to surface tension. To enable correlation of applied pressure with infiltration kinetics, the capillary pressure drop, ΔP_γ, must be known. According to the theory presented in Reference 1 (Eqs. [47], [51], [58], and [60]), a plot of $\psi^2 = L^2/t$ as a function of ΔP_T (*i.e.*, $P_T - P_g$) should be linear at zero metal superheat, with its intercept on the abscissa axis equal to ΔP_γ (Eq. [47] with $\chi_s = 0$). With a low superheat, such as 20 K for aluminum, the deviation from linearity is small. In Figure 6, L^2/t is plotted for a series

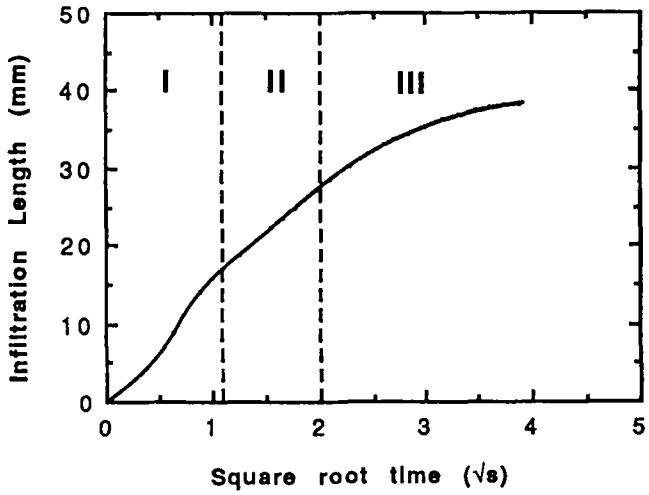

Fig. 5—Typical plot of length *vs* square-root time showing regions I, II, and III discussed in the text. This particular curve is from run 8, Table I.

of runs with low superheat and identical values of all parameters except for the applied pressure ΔP_T. A straight line through these data points intersects the abscissa at approximately 1 MPa, and this is the value used for ΔP_γ in the calculations that follow. This approximate value is corroborated by the observation that at applied pressures at or below 0.9 MPa, no or very little infiltration of the preforms was observed (Table I, runs 1, 2, 3, and 27). Given the relatively small range of fiber volume fraction explored in this work, we ignore variations in ΔP_γ with fiber volume fraction and use the constant value of $\Delta P_\gamma = 1$ MPa in all applications of equations derived in Reference 1.

Figures 7 through 13 are plots of data from Table I and show comparisons of these data with curves calculated using the analysis of Reference 1. Table II summarizes the values of thermal and physical constants used in the calculations.

Solution of the equations also required a value for the fiber radius, r_f. Fibers in the preforms used in this investigation ranged mostly from 0.75 to 2.5 μm in radius, with a nominal value reported to be ~1.5 μm. In order to assign a single value for fiber radius, we measured the permeability of the preforms to water using standard techniques[2] and calculated the resulting apparent fiber radius from Eq. [26] of Reference 1. This yielded an apparent fiber radius of 1.9 μm, satisfactorily close to the nominal value of 1.5 μm reported by the supplier. Thus, we used $r_f = 1.9$ μm when applying equations derived in Reference 1.

The curves drawn in Figures 7 through 13 were calculated from Eqs. [47], [51], [56], [58], and [60] of Reference 1. The values of fiber volume fraction, fiber temperature, and metal temperature were taken directly from the processing parameters of each experiment (Table I).

The influences of fiber volume fraction and fiber temperature are shown in Figures 8 and 9, respectively. The sensitivity of the kinetics of preform infiltration to fiber volume fraction is a result of the dual role of an increasing fiber volume fraction in decreasing the spacing between fibers and in increasing the amount of solid formed per unit volume of preform. This dual effect significantly decreases the permeability for a relatively small increase in fiber volume fraction.

The effect of metal superheat is shown in Figure 10. Metal superheat is seen to play a minor role in the effect

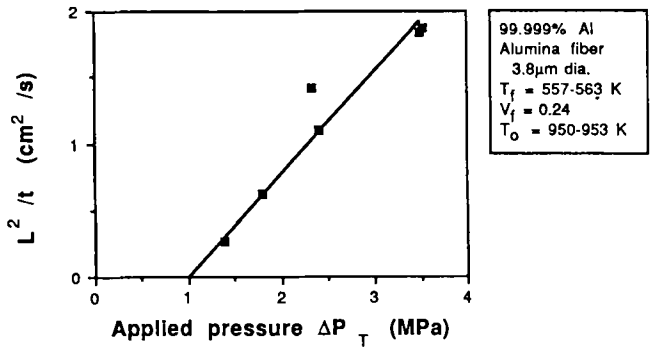

Fig. 6—Experimental values of infiltration kinetics as a function of total applied pressure.

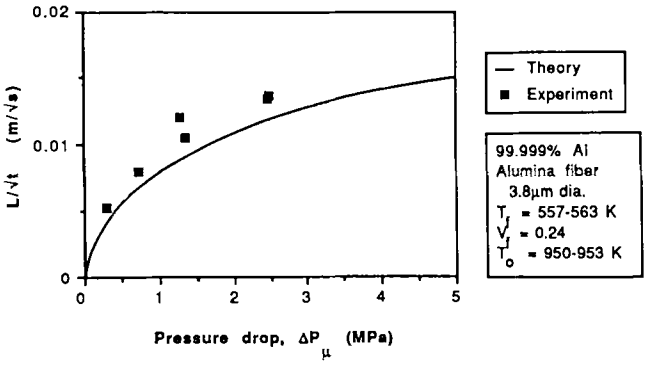

Fig. 7—Effect of pressure drop on $L/\sqrt{t}$; the theoretical curve drawn is for 20 °C of superheat, and was calculated from Eqs. [47], [51], [58], and [60] of Ref. 1. Experimental data are plotted with the assumption that the capillary pressure drop at the infiltration front is 1 MPa.

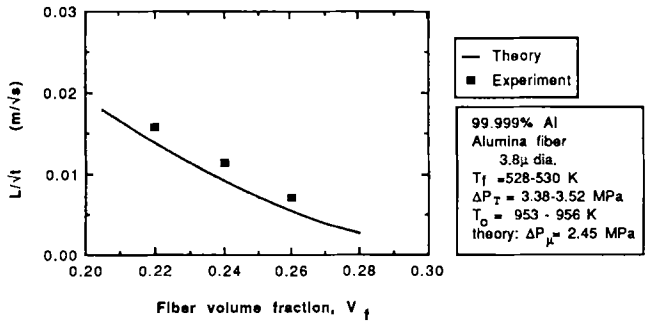

Fig. 8—Effect of fiber volume fraction on $L/\sqrt{t}$; curve drawn is for 20 °C of superheat.

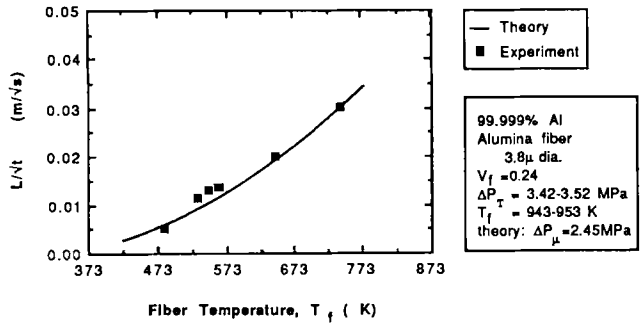

Fig. 9—Effect of fiber temperature on $L/\sqrt{t}$; curve drawn is for 20 °C of superheat.

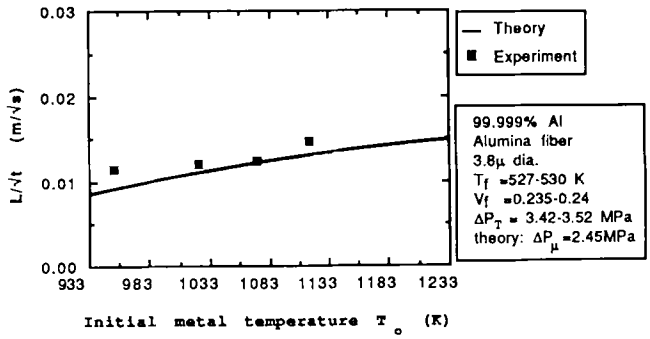

Fig. 10—Effect of metal superheat on $L/\sqrt{t}$.

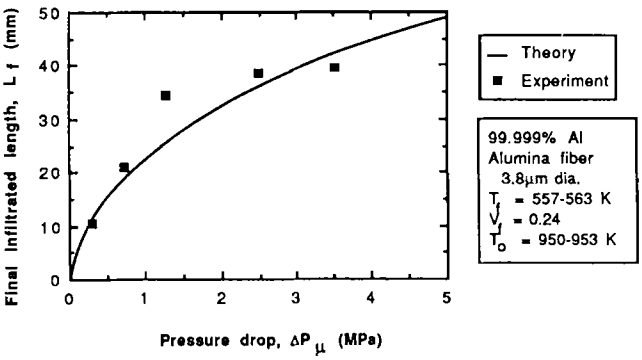

Fig. 11—Effect of pressure drop on final infiltrated length. Calculations assume h_e = 200 W/m^2 K.

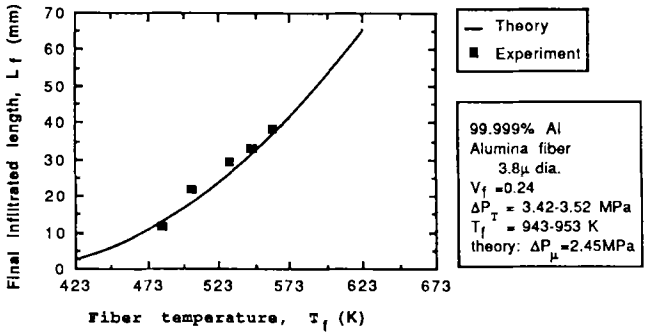

Fig. 13—Effect of fiber temperature on final infiltrated length. Theoretical curve assumes h_e = 200 W/m^2 K.

on infiltration kinetics, in agreement with results from our model. This is because to impart a significant effect on overall permeability, a considerable portion of the composite must be remelted. Remelting of aluminum requires a large amount of energy, which is not obtained for metal superheats normally encountered in foundry practice (at most 200 K), so remelting distances are moderate and the effect on infiltration kinetics is minimal.

Using the aluminum-lead experiments as a verification of the role of superheat, the optical micrograph in Figure 14 shows the results for metal with 60 K superheat. Note the existence of a region at the base of the composite where the aluminum was entirely replaced by lead. At the end of the experiment, therefore, this region was entirely liquid; any aluminum which had solidified was remelted. In the central portion of the composite, lead and aluminum coexist in the matrix, indicating that some aluminum was retained by the fibers as the lead flowed past. To be retained by the fibers, this aluminum must have been solid. It is also evident from this figure that fingering occurred at the remelting front (*i.e.*, the planar remelting front was unstable, resulting in cells or "fingers" of fully liquid matrix composite protruding into the partly solid matrix composite), analogous to observations on fluid displacement in porous media.[4]

Indication of a two-zone structure in cast aluminum matrix composites was observed when the superheat was sufficiently high to yield a region of large columnar grains in the upstream portion of the composite (Figure 15). Note that this is also experimental evidence that the fibers do not act as nucleation sites for the growth of solid

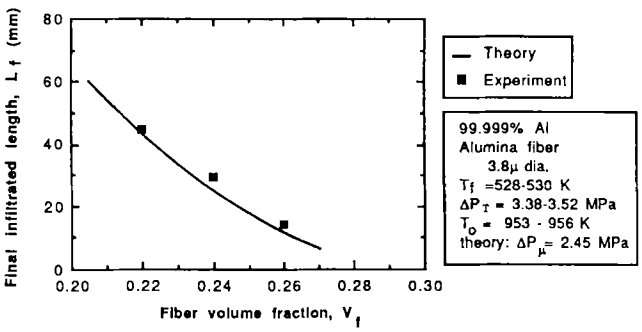

Fig. 12—Effect of fiber volume fraction on final infiltrated length. Theoretical curve assumes h_e = 200 W/m^2 K.

metal. A microstructure taken further downstream in the same sample and in the vicinity of the infiltration front is shown in Figure 16, where many orientations of etch pits in a small volume indicate a fine-grained matrix. This is a consequence of the high nucleation rate achieved by rapid cooling by the fibers at the infiltration front.

The curves of final infiltration length, shown in Figures 11 through 13, were calculated from Eq. [34] of Reference 1. As a first approximation, the external heat loss was assumed to be limited by convection to the surroundings and described by a single heat transfer coefficient, h_e, between the sample and its surroundings at the fiber preheat temperature. Thus, the growth of solid from the mold wall was calculated by Eq. [65] of Reference 1. The best agreement of theory with experiment was obtained by assuming 200 W m^{-2} K^{-1} for h_e. Although agreement with all experimental data using a single value for h_e is satisfactory, a more detailed analysis would be necessary to account for the complexity of heat transfer from the sample to the mold and its surroundings, consisting of successive layers of insulating material, a furnace, and pressurized gas. The value of h_e of 200 W m^{-2} K^{-1} is satisfactory, however, in that it lies between the typical values of 3000 W m^{-2} K^{-1} observed in casting fluidity experiments with aluminum, where all heat was extracted into a quartz mold wall,[5] and 10 W m^{-2} K^{-1} for cooling by natural convection in air.[6] Using the above value of h_e, it is seen that the effects of the processing parameters on L_f mirror those of $L/\sqrt{t}$, with the same experimental agreement with theory. The curves are calculated for the case of no metal superheat; the theory has not been extended to predict the effect of metal superheat on final infiltrated length, which was found experimentally to be small.

The calculation of L_f is based upon the assumption that external heat losses are responsible for the cessation of infiltration. The physical model of solidification from the mold wall is confirmed by a reexamination of the aluminum-lead experiment of Figure 14. Near the mold wall, the matrix is aluminum, indicating complete solidification of the aluminum at the mold wall prior to infiltration by lead. This corresponds to region 2 of the discussion in Reference 1. Figure 14 of this paper is to be compared with Figures 1 and 11 of Reference 1.

The effect of the mold radius is shown experimentally in Figure 17. Note that a change in mold radius does not influence the infiltration profile during the early stages of infiltration, but it does have an influence on the total

Table II. Values of Selected Thermal and Physical Constants

Property	Units	Aluminum[13]	SAFFIL[14]	Quartz[15]	Air[16]
ρ	(kg/m^3)	2.4×10^3	3.3×10^3	2.2×10^3	1.1×10^0
ρC	(J/m^3 K)	2.6×10^6	4.0×10^6	3.1×10^6	1.1×10^3
k	(W/m K)	93	8	2	2.6×10^{-2}
α	(m^2/s)	36×10^{-6}	2×10^{-6}	0.65×10^{-6}	2.4×10^{-5}
$\rho \Delta H$	(J/m^3)	9.5×10^8	—	—	—
μ	(Pa · s)	1.3×10^{-3}	—	—	—

time of flow. Theoretically, the mold radius should influence only the external heat loss kinetics and not the interaction between the metal and fibers which is accounted for in the adiabatic model of Reference 1. Therefore, the slopes of the infiltration profiles during the early stages of infiltration will remain unchanged for the two different mold radii, while the final infiltration lengths will increase as the mold radius increases, as confirmed experimentally by data in Figure 17 for 99.9 wt pct pure aluminum.

Metal purity was noted to have a very strong effect on the infiltration kinetics, as shown in Figure 18. Not only was there a pronounced difference in flow behavior between 99.999 and 99.9 wt pct aluminum, but when repeatedly using a melt of 99.999 wt pct aluminum, a significant effect on infiltration kinetics was detected when the melt purity dropped to only 99.95 wt pct. The effect of metal purity on results of a vacuum casting fluidity test was studied by Feliu *et al.*,[7] who reported an 8 pct decrease in fluidity when changing from 99.99 to 99.9 wt pct aluminum. They concluded that the impurities influenced the mode of solidification, which, in turn, affected the drag between the liquid and stationary solid metal. This conclusion has also been supported by observations of the transition from planar to cellular solidification interfaces due to small changes in solute levels.[8] Therefore, it is plausible that the lower purity metal does not initially solidify at the infiltration front in a form that approximates that of a smooth cylinder surrounding the fibers, but solidifies following a different morphology, which is probably more akin to what is observed when an alloy solidifies in the presence of fibers after infiltration.[9,10] These data confirm conclusions in our previous publication[11] on infiltration by 99.9 wt pct aluminum,

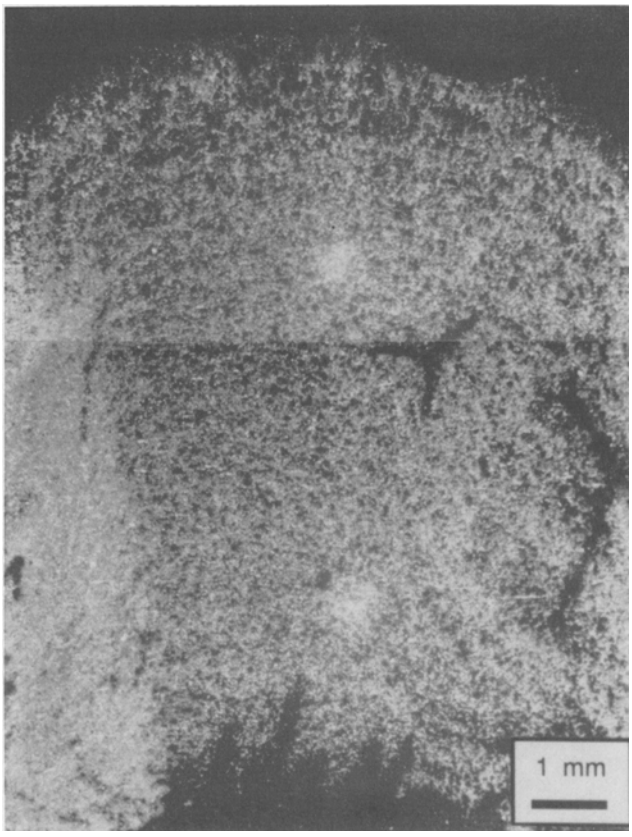

Fig. 14—Optical micrograph of a cross section of a sample infiltrated by aluminum followed by lead. Dark regions are lead or fiber, and light regions are aluminum. Infiltration occurred upward. Infiltration parameters were $V_f = 0.23$, 99.9 pct pure Al, $T_f = 608$ K, $T_0 = 993$ K, $\Delta P_T = 3.5$ MPa; sample diameter was 11 mm.

Fig. 15—Optical micrograph of the preform entrance region of etch-pitted SAFFIL alumina-fiber-reinforced 99.9 pct pure aluminum matrix composite viewed under crossed polarizers in the optical microscope. Large columnar grains are visible (in white) in this region. The preform entrance is at the bottom of the figure, and infiltration occurred upward. Horizontal striations are due to delamination of the preform.

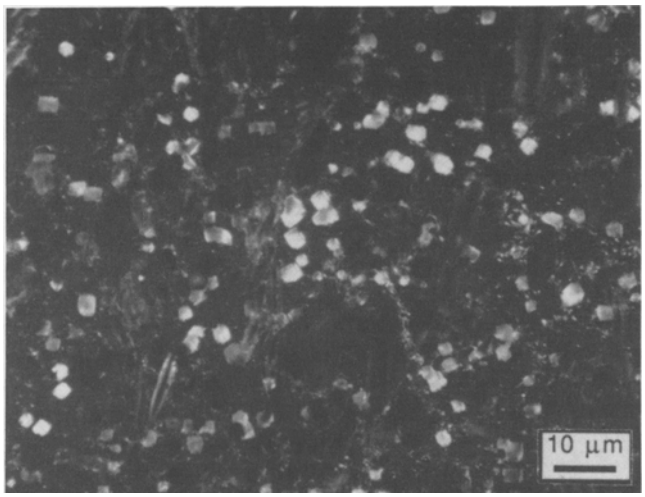

Fig. 16—Photomicrograph of the same sample as in Fig. 15, viewed as before but at higher magnification. This micrograph was taken farther away from the preform entrance, closer to the infiltration front, above the region in Fig. 15. Here, etch pits display a variety of orientations over a much smaller area of composite (many etch pits are in white and thus distinguishable from fibers and the rest of the matrix), denoting a grain size on the order of 10 μm, close to the infiltration front.

wherein discrepancies between our results and those of Fukunaga *et al.* were attributed to a difference in metal purity.

IV. VALIDITY OF ASSUMPTIONS

In what follows, each of the main assumptions introduced in the theory of Reference 1 is briefly justified for the system investigated here. Table II is a list of the physical and thermal properties for the SAFFIL-reinforced aluminum composites studied in these experiments.

Cross flow through a square array of cylinders: It was observed that even though the infiltration front features numerous fine spikes on a microscopic scale, on a macroscopic scale as measured in these experiments, the infiltration front progresses as a plane, a short distance behind which all pores in the preform are filled. The "slug-flow" assumption of Reference 1 is thus justified.

Data in the review of Jackson and James[12] indicate that the geometry of the fibrous arrays is not a significant factor for the measurements of their permeability as long as flow of the metal is perpendicular to the fiber axes.

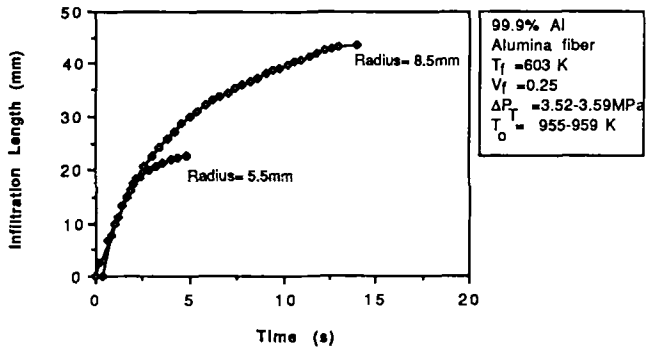

Fig. 17—Effect of mold radius on infiltration behavior.

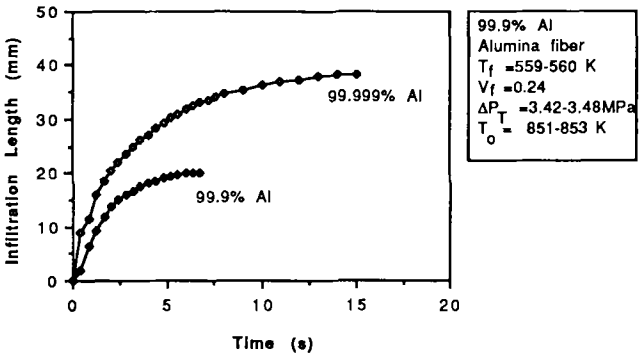

Fig. 18—Effect of metal purity on infiltration behavior.

This was the case for the vast majority of the fibers in the SAFFIL preforms.

Darcy's law: Throughout this work, it is assumed that Darcy's law describes the flow of metal through the preform. As discussed in Appendix I of Reference 1, this constitutes a valid assumption for Reynolds numbers less than 1. In these experiments, the maximum velocity measured is on the order of 0.01 m/s. This yields a Reynolds number on the order of 0.08, clearly within the region of validity of Darcy's law.

Negligible heat transfer ahead of the infiltration front: The effect of thermal losses ahead of the infiltration front is described in detail in Reference 1. Referring to Figure 8 of the same reference, this effect is significant only when the value of B (defined in Eq. [43]) falls below unity. For the values of $\psi = L/\sqrt{t}$ encountered in experiments reported here, B is always greater than 10. The effect of heat transfer ahead of the infiltration front is therefore negligible for all the experiments considered in this work.

Negligible temperature gradients over the composite sample diameter perpendicular to the infiltration direction in the presence of external cooling: We assume that the rate of heat extraction at the mold wall is limited by convection to a surrounding medium at temperature T_f, the initial fiber temperature. The Biot number gives a measure of the significance of temperature gradients within the composite, defined as:

$$\mathrm{Bi} = \frac{h_e R_i}{k_c}$$

where h_e is the interfacial heat transfer coefficient between the metal and mold, R_i is the inside radius of the mold, and k_c is the thermal conductivity of the composite. The assumption of negligible temperature gradients across the sample diameter is consistent with the value for h_e derived from experimental data, which yields Bi = 0.03.

V. SUMMARY AND CONCLUSIONS

1. An apparatus was designed and built for the infiltration of molten metal into porous preforms under controlled processing conditions. The apparatus utilized pressurized gas to cause infiltration under a constant applied pressure.

2. A sensor was developed to measure the flow of liquid metal through a porous preform composed of nonconductive material. This sensor was used for quantitative measurements of infiltration kinetics.
3. Quantitative agreement of theory with experimental values of infiltration kinetics and final infiltrated length has been shown under a variety of processing conditions. For example, it was shown that an increase in fiber volume fraction of only 10 pct from 0.22 to 0.24 caused a drop in infiltration length of 46 pct, and an increase in fiber temperature by 10 pct from 523 to 553 K increased infiltration length by 35 pct. The effect of applied pressure on infiltration length is parabolic after correction for the capillary pressure drop at the infiltration front; doubling the pressure that drives fluid flow results in a $\sqrt{2}$ increase in infiltrated length.
4. Metal superheat induces a gradual remelting at the preform entrance of solid previously formed. This mechanism was verified by metallographic observation of experiments performed with the immiscible aluminum-lead system. The technique also provided experimental verification for solidification from the mold walls, which is the mechanism for cessation of infiltration.
5. The effect of metal purity on infiltration was extremely pronounced. A decrease in purity from 99.999 to 99.9 wt pct resulted in a decrease in infiltration length of 50 pct. This observation is interpreted by assuming that the impurity level affects the mode of solidification; the assumption that the metal solidifies as a smooth sheath surrounding the fibers is no longer consistent with infiltration kinetics.
6. These experimental results provide confirmation of the analysis of infiltration of metal matrix composites presented in Reference 1. Therefore, it is suggested that physical models for the infiltration process of three-dimensional shapes proposed in that work can be used with some degree of confidence in the analysis of more complex preform and mold geometries. Numerical techniques would be required for solution of most of these cases.

ACKNOWLEDGMENTS

This work was sponsored by the Innovative Science and Technology Division of the Strategic Defense Initiative Office (SDIO) through the Office of Naval Research, Contract No. N00014-85-K-0645, under the supervision of Dr. S.G. Fishman and, in its initial stage, by General Motors Corporation. Support from ALCOA and Toyota Corporation in the form of two endowed chairs at MIT (AM and MCF) is also gratefully acknowledged. We are also grateful to our reviewers for their thoroughness and the many helpful comments we received.

REFERENCES

1. A. Mortensen, L.J. Masur, J.A. Cornie, and M.C. Flemings: *Metall. Trans. A*, 1989, vol. 20A, pp. 2535-47.
2. T.W. Lambe and R.V. Whitman: *Soil Mechanics*, S.I. Version, John Wiley & Sons, New York, NY, 1979, p. 281.
3. *Smithells Metals Reference Book*, 6th ed., Butterworth's, London, 1983, pp. 10-27.
4. A.E. Scheidegger: *The Physics of Flow through Porous Media*, 3rd ed., University of Toronto Press, Toronto, 1974, pp. 229-39.
5. M.C. Flemings, F.R. Mollard, E. Niyama, and H.F. Taylor: *Trans. Am. Foundrymen's Soc.*, 1962, vol. 70, pp. 1029-39.
6. J. Szekely and N.J. Themelis: *Rate Phenomena in Process Metallurgy*, John Wiley & Sons, New York, NY, 1971, p. 234.
7. S. Feliu, M.C. Flemings, and H.F. Taylor: *The British Foundryman*, 1960, vol. 43, pp. 413-25.
8. W.A. Tiller and J.W. Rutter: *Can. J. Phys.*, 1956, vol. 34, pp. 96-121.
9. A. Mortensen, J.A. Cornie, and M.C. Flemings: *Metall. Trans. A*, 1988, vol. 19A, pp. 709-21.
10. A. Mortensen, M.N. Gungor, J.A. Cornie, and M.C. Flemings: *J. Met.*, Mar. 1986, vol. 38, pp. 30-35.
11. L.J. Masur, A. Mortensen, J.A. Cornie, and M.C. Flemings: *Proc. 6th Int. Conf. Composite Materials (ICCMVI)*, F.L. Matthews, N.C.R. Buskell, J.M. Hodgkinson, and J. Morton, eds., Elsevier Applied Science, London, 1987, pp. 2.320-2.329.
12. G.W. Jackson and D.F. James: *Can. J. Chem. Eng.*, 1986, vol. 64, pp. 364-74.
13. *Smithells Metals Reference Book*, 6th ed., Butterworth's, London, 1983, pp. 8.1, 14.7, 14.10.
14. Imperial Chemical Industries SAFFIL Data Sheet, 1984.
15. *CRC Handbook of Chemistry and Physics*, 56th ed., 1975, p. F-78.
16. *CRC Handbook of Chemistry and Physics*, 56th ed., 1975, p. F-13.